




Cite this: *RSC Adv.*, 2023, 13, 5107

# Electrochemical stripping voltammetrical sensor based on polypyrrole exfoliated polyetheramine–montmorillonite nanocomposite for nanomolar detection of nifuroxazide†

Mona Elfiky, \* Mohamed Ghoneim, Hanaa El-Desoky, Amara Hassanein and Nehal Salahuddin 

A series of polypyrrole/polyetheramine–montmorillonite nanocomposites have been fabricated by the intercalation of different types of polyoxyalkylene amine hydrochloride (Jeffamines: D<sub>400</sub>, D<sub>2000</sub>, T<sub>5000</sub>, and T<sub>403</sub>) into montmorillonite layers *via* the cation-exchange process followed by *in situ* polymerization of pyrrole. The physicochemical characteristics of as-prepared nanocomposites were investigated using Fourier transform infrared (FT-IR), X-ray diffraction (XRD), scanning electron microscopy (SEM), transmission electron microscopy (TEM), Brunauer–Emmett–Teller (BET), and electrochemical impedance spectroscopy (EIS) instruments. The change of the types of Jeffamine causes a change in the geometrical structure, and surface area of nanocomposites. Noteworthy, the resulting polypyrrole/D<sub>2000</sub>–montmorillonite (PDM-50) nanocomposite exhibited a cauliflower-like shape with a specific surface area (116.2 m<sup>2</sup> g<sup>−1</sup>) with the highest conductivity. Furthermore, the modified stripping voltammetric carbon paste sensor was fabricated based on 1.0% [PDM-50] nanocomposites to detect the drug nifuroxazide (NF). The sensor achieved detection limits (LD) of 0.24, and 0.9 nM of NF in the medication, and human urine fluid, respectively. This sensor showed appropriate repeatability, reproducibility, stability, and selectivity for NF sensing in different fluids accompanied by other interferents.

Received 30th September 2022  
Accepted 21st January 2023

DOI: 10.1039/d2ra06160k

rsc.li/rsc-advances

## 1. Introduction

4-Hydroxy-N'-[(5-nitrofur-2-yl)methylene]benzohydrazide (nifuroxazide (NF))<sup>1</sup> is an oral nitrofurantoin antibiotic, with a wide range of bactericidal activity against Gram-positive and Gram-negative entero-pathogenic organisms (Scheme S1†). NF is extensively used as an intestinal antiseptic in the treatment of susceptible gastrointestinal infections.<sup>2</sup> But NF is not absorbed from the gastrointestinal tract and, consequently rapidly removed from the body without metabolism. Due to the therapeutic significance of the NF, various analytical systems have been applied to evaluate its validity in commercial and biological fluids.<sup>2–25</sup> It is noteworthy that the two spectrofluorimetric methods<sup>3,4</sup> allow NF to be detected in either a single form or in a binary mixture with drotaverine. However, the drawback of the former<sup>3</sup> is that the method can not be applied for the determination of NF in presence of drotaverine, since the alkaline conditions required would lead to degradation of drotaverine<sup>4</sup> and thus the method requires intensive

sample pretreatment.<sup>4</sup> Furthermore, most reported methods<sup>2,5–12,15</sup> were successfully applied for analysis of NF in its dosage forms with no attempt for its assay in biological fluids. Only one HPLC method<sup>15</sup> was applied to measure NF concentrations (down to 7.27 nM), which were extracted from buffered plasma with chloroform. However, the required high-strength ionic buffered mobile phases are hazardous for column efficiency and need prolonged time for column saturation and washing as well as insufficient sensitivity and selectivity.

In contrast, the electrochemical sensors have higher sensitivity and proper selectivity in the field of analytical applications without the need for complex sample preparation with a short analysis time.<sup>26–30</sup> The recent reports describe the detection of NF in commercial products (capsules and tablets) *via* differential pulse polarographic (DPP), biological fluids (urine and human serum) *via* adsorptive stripping voltammetry (AdSV) upon mercury, and carbon paste sensors.<sup>27,30</sup> Also, the electro-oxidation of NF was investigated *via* differential pulse voltammetry (DPV) upon bare, and Sephadex-modified carbon paste sensors with LOD of 20 nM; this direct detection of NF in urine is not efficient upon unmodified and modified sensors due to the large oxidation peak of blank urine. Recently, J. D. Mozo *et al.*<sup>29</sup> has been successfully achieved LOD 10 ng mL<sup>−1</sup> in a bulk form *via* linear-sweep adsorptive stripping voltammetry (LS-

Department of Chemistry, Faculty of Science, Tanta University, 31527, Egypt. E-mail: Elfiky\_mona@science.tanta.edu.eg; Fax: +20403350804; Tel: +201004155414

† Electronic supplementary information (ESI) available. See DOI: <https://doi.org/10.1039/d2ra06160k>



AdSV) upon a screen-printed carbon nanofiber modulated sensor, and revealed an average recovery of  $100.7 \pm 2.5\%$  in commercial tablets.<sup>29</sup> Therefore, the modification of sensor has a great importance in electrochemistry as they enhance the sensitivity of specific analytes.

Montmorillonite (MMT) is natural clay, which is one of the very promising modifiers, which belongs to the smectite group of clays with a layer lattice. MMT has a high chemical, mechanical stability, a well-layered structure, and strong adsorptive properties attributed to the expandability of the internal layers. Moreover, the SW-AdSV method has been well characterized as an extremely sensitive source for electroanalytical applications of ultra-trace determinations of a variety of organic or inorganic substances.<sup>31–33</sup> However, to date no square-wave adsorptive anodic stripping voltammetric (SW-AdASV) method is available in the literature for the determination of NF using a modified CPE with Na-MMT clay.

Also, slices of MMT clay can interact with different guest species including metal oxides to form hybrids,<sup>31</sup> or/and conducting polymers to form nanocomposites<sup>34</sup> with different morphologies for different sorts of applications. Notably, MMT clay was successfully used as a modified material to improve the adsorptive behaviour of the carbon paste sensor (CPS) for the electrochemical sensing of some inorganic materials.<sup>31,35,36</sup> However, the usage of clays in electrochemical applications is limited due to their poor electrical conductivity.<sup>37</sup> Furthermore, the organophilic MMT (OMMT) could be fabricated *via* the ion-exchange process of organic compounds (e.g., surfactants and multifunctional organic amines chains), resulting in stable OMMT with powerful adsorption, and considerable dispersibility in organic dispersion medium.<sup>38–40</sup> Various reports have been made to modify MMT with different types of poly(oxypropylene)amines;<sup>41–44</sup> the resulting material showed potential use in various applications, such as a curing agent for epoxy,<sup>45,46</sup> and drug-delivery vehicles.<sup>47</sup>

On the other hand, scientific innovations have recently gained extensive attention to the usage of polypyrrole (Ppy) in electrochemical sensing applications<sup>48,49</sup> due to its excellent conductivity up to  $1000 \text{ S cm}^{-1}$ , and environmental stability.<sup>32,48</sup> Recently, many research efforts have been made to prepare montmorillonite/polypyrrole (MMT/Ppy) nanocomposites.<sup>50–54</sup> But, to achieve a better degree of miscibility with the polymer matrix, it is essential to adjust them with organic cations to improve their hydrophobicity. In addition, some functional organic cations can react with the polymer matrix.<sup>55,56</sup> N. Salahuddin *et al.*,<sup>57</sup> have fabricated nanocomposites with higher resistivity, and hydrophobicity in comparison with pristine polyurethane; the syncretization was carried out *via in situ* polymerization of toluene diisocyanate and butanediol with different content of OMMT. As well, Doris Pospiech *et al.*<sup>58</sup> studied the dispersion property of MMT/poly(oxyalkylene)s in polypropylene. Recently, Dos Santos *et al.*<sup>59</sup> has used polyester-based thermoplastic polyurethane (TPU) as matrix and Ppy or MMT/Ppy composite in the presence of surfactant to fabricate polymer composites *via* melt mixing technique.

Herein, a series of polypyrrole/polyetheramine–montmorillonite [Ppy/organoclay] nanocomposites were fabricated by

intercalation of various molecular masses of polyoxyalkylene amine hydrochloride (Jeffamine D<sub>400</sub>, D<sub>2000</sub>, T<sub>403</sub>, and T<sub>5000</sub>) (Scheme S2†) into Na-MMT *via* ion-exchange treatment followed by the *in situ* polymerization of Py with different organoclay contents. Afterward, sensitive electrochemical sensors based on CP blended with the prepared nanocomposites were fabricated and examined to detect NF using square-wave adsorptive anodic stripping voltammetry (SW-AdAS) in commercial, and human urine fluid.

## 2. Experimental

### 2.1. Materials, equipments, electrochemical liquids, and fabrication of unmodified and modified CPSS

All details are mentioned in the ESI† section.

### 2.2. Preparation of polyetheramine–montmorillonite

The polyetheramine–montmorillonite (organoclay) was synthesized *via* cation-exchange process between the Na<sup>+</sup> in the MMT matrix and  $-\text{NH}_3^+$  groups in Jeffamine. 5 g of MMT was swelled in 300 mL distilled water (DW) with steady stirring for 3 h at 60 °C and for 24 h at 25 °C. 6.2 g of acidified Jeffamine D<sub>2000</sub> with an aqueous solution of HCl was inserted into the swelled clay solution with steady stirring for 24 h. The precipitate was thoroughly rinsed with DW until no Cl<sup>−</sup> ions were detected. The precipitate of (D<sub>2000</sub>-MMT) was dried at 60 °C to give 8.191 g. The same procedure was carried out to prepare other types of organoclay, as listed in Table 1.

### 2.3. Preparation of Ppy and Ppy/polyetheramine–montmorillonite nanocomposites

(0.98 g, 0.14 M) of Py was added into 50 mL HCl (0.1 M). Then, 0.29 M of FeCl<sub>3</sub> (7.8 g dissolved in 50 mL HCl, 0.1 M) was inserted into Py solution dropwise with steady stirring for 24 h. The molar ratio between Py and FeCl<sub>3</sub> was (1 : 2). The precipitate was thoroughly rinsed with DW, and dried at 70 °C for 24 h in a vacuum oven. 0.1 g of D<sub>2000</sub>-MMT was stirred in 5 mL DMF for 24 h, and 3 h at 60 °C. Then, 0.29 M of FeCl<sub>3</sub> (7.8 g dissolved in 50 mL HCl, 0.1 M) was inserted into the organoclay suspension with constant stirring for 24 h. The Py (0.98 g, 0.14 M) dissolved in 50 mL HCl (0.2 M), and was added into the organoclay solution dropwise with constant stirring for 24 h at 30 °C. Finally, the nanocomposite precipitate was thoroughly rinsed with DW and dried at 60 °C in the oven for 48 h to afford 0.7424 g of [PDM-10]. The same procedure was carried out to

Table 1 Composition data of different types of organoclay

Code	Jeffamine		MMT wt (g)	Yield wt (g)
	Type	Wt (g)		
D <sub>2000</sub> -MMT	D <sub>2000</sub>	6.2	5	8.2
D <sub>400</sub> -MMT	D <sub>400</sub>	1.4	5	5.6
T <sub>5000</sub> -MMT	T <sub>5000</sub>	11.6	5	7.9
T <sub>403</sub> -MMT	T <sub>403</sub>	1.0	5	5.6



prepare different types of nanocomposites with different contents of organoclay, as listed in (Table S1†).

### 3. Results and discussion

#### 3.1. FTIR and XRD

FTIR spectra of Na-MMT, organoclay, Ppy, and Ppy/organoclay nanocomposites with different content of organoclay were illustrated in (Fig. S1(a-d)†). The spectrum of Na-MMT displayed absorption bands at 3633, and 1050  $\text{cm}^{-1}$ , which could be attributed to the stretching vibration of Al-OH, and Si-O-Si, respectively.<sup>60</sup> While bands at 1635, 921, and 523  $\text{cm}^{-1}$  are ascribed to bending of Al-OH, Al-Al-O, and Si-O-Al respectively. The FT-IR spectrum of D<sub>2000</sub>-MMT displayed a shift in the band at 1658, and 1485  $\text{cm}^{-1}$ , which could be corresponded to the asymmetrical and symmetrical bending of N-H in  $\text{NH}_3^+$ , affirming the electrostatic attraction between silicate sheets and polyoxypropylene.<sup>61</sup> Furthermore, the spectrum of Ppy exhibited bands at 1543, 1456, 1168, and 1046  $\text{cm}^{-1}$ , which could be assigned to the stretching C=C, stretching of C-N, C-C in-plane deformation, and bending of N-H in Py rings, respectively.<sup>62</sup> On the other hand, the spectrum of [PDM] displayed the band of the C-C stretching of Ppy at 1543  $\text{cm}^{-1}$ . Notably, the N-H stretching band shifted from 3422 to 3441  $\text{cm}^{-1}$  for [PDM-

50] confirming the interaction between sheets of MMT and Ppy matrix.<sup>63,64</sup> The same results were observed for other nanocomposites.

XRD patterns of Na-MMT, Ppy, organoclay, and Ppy/organoclay nanocomposites were shown in (Fig. 1(a-d)) at various organoclay contents. In the XRD pattern of Ppy, the broad band at  $2\theta = 18.3^\circ$  corresponded to the amorphous crosslinked chains of the polymer matrix.<sup>48</sup> The crystalline band corresponds to *d*-spacing between layers ( $d_{001}$ ) in the pristine clay sample 9.6 Å was shifted after preparation of organoclay, owing to the intercalation of polyoxyalkylene between the sheets of MMT.<sup>65</sup> The diffraction patterns displayed in (Fig. 1) indicate a regular lattice spacing of 20.1 Å for D<sub>2000</sub>, 15.2 Å for D<sub>400</sub>, 14.0 Å for T<sub>500</sub>, and 14.5 Å for T<sub>403</sub> and with an expansion of the clay galleries by 10.8, 4.9, 4.89, and 5.2 Å respectively. Furthermore, Ppy/organoclay nanocomposites with 10, 20, and 50% of organoclay show no distinguishable band in the XRD pattern, confirming the exfoliation of the organoclay during the *in situ* polymerization of Py. While the polymerization of Py within D<sub>2000</sub>-MMT, D<sub>400</sub>-MMT, and T<sub>403</sub>-MMT 50 a broad  $d_{001}$  was observed, which could be related to the partially exfoliated structure.<sup>65</sup> It should emphasize that Ppy is more adequate to intercalate between clay sheets modified by T<sub>5000</sub> even at high

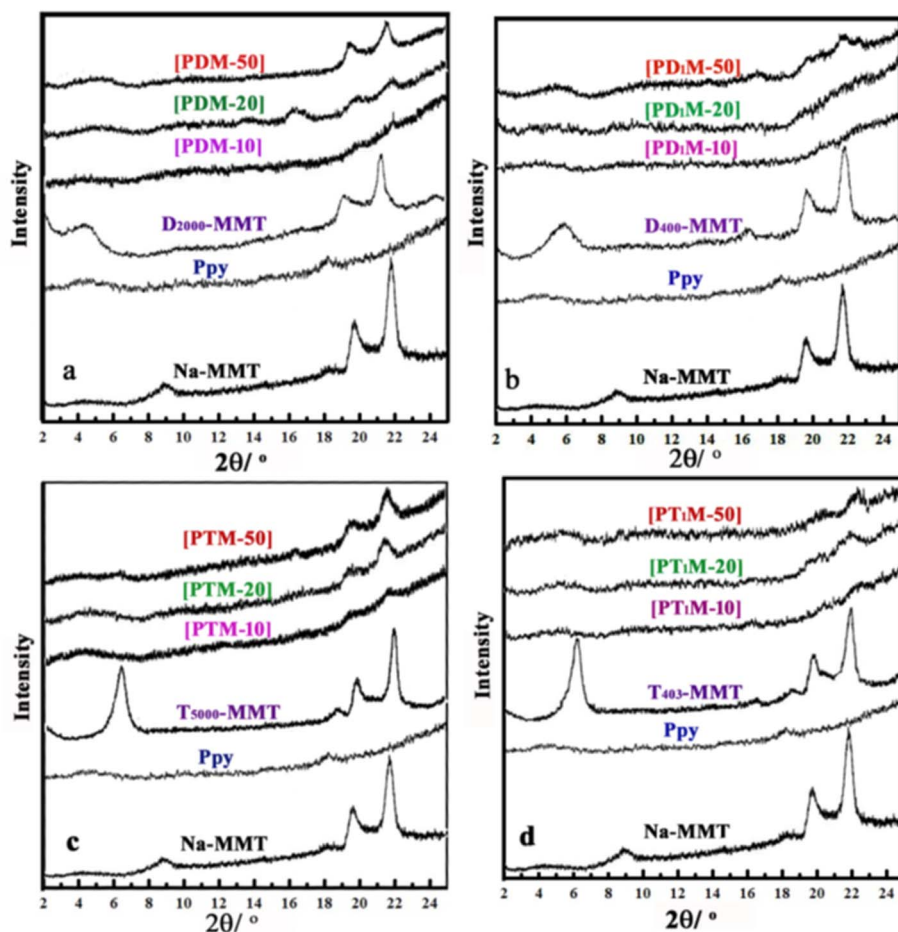


Fig. 1 X-ray diffraction pattern of Na-MMT, Ppy, organoclay, and Ppy/organoclay nanocomposites at different content of organoclay.



concentrations. The disappearance of the basal reflection indicates the formation of an exfoliated nanostructure.

### 3.2. The preliminary electrochemical sensing test and SEM micrographs of the surface of sensors

AdAS-SW voltammograms of 30.0 nM NF in pH 5 (B-R buffer) were evaluated upon [B], 7.0% [Na-MMT], and 1.0% of various nanocomposites MCPSS at  $E_{acc} = 0.6$  V vs., Ag/AgCl/KCl for 10 s, as shown in (Fig. S2(a)†). The maximal peak was obtained upon the 1.0% [PDM-50] MCPSS with about 7- and 2.7-time increase compared with [B], and 7.0% [Na-MMT] CPSs, respectively. Whereas, the organoclay was obtained *via* a simple ion-exchange process of hydrophilic MMT with polyoxyalkylene amine, leading to opening up the lamellae of MMT and causing profound changes in the sorption and/or intercalation of organic molecules including drug.<sup>66,67</sup> The adsorption of the drug increases with increasing the hydrophobicity of nanocomposites. Whereas longer organo-chains (*e.g.*, Jeffamine D<sub>2000</sub>, and T<sub>5000</sub>) have more active sites available for adsorption and are more hydrophobic than shorter chains.

In general, the change in the sensitivity of sensors could arise from the significant difference in the geometrical structure of the surface of sensors accompanied by improvement in the conductivity. As demonstrated in (Fig. 2), SEM micrographs of the surface of 1.0% [PT<sub>1</sub>M-50] (Fig. 2(a)), and [PTM-50] (Fig. 2(b)) MCPSS appeared as smooth domains assembled in small necklace-like structure. As well, 1.0% [PT<sub>1</sub>M-50] MCPSS has compact particles relative to [PTM-50] MCPSS, which shows more voids to improve the adsorption of NF upon its surface. Furthermore, the morphological structure of 1.0% [PDM-50] MCPSS (Fig. 2(c)) shows irregular granular structures with long coral reefs-like shapes as well as more voids and vacuoles,

providing the largest surface area of CPS and more improvement in the adsorption, and sensitive detection of NF compared with the other MCPSSs.

### 3.3. The conductivity and morphological properties of nanocomposites

The high conductivity of nanocomposites refers to the relatively slow rate of Ppy polymerization in the presence of organoclay, which may promote the higher-ordered morphology of Ppy with limited defects. Therefore, the preliminary investigation of the electrical conductivity of all prepared materials was carried out as a function of Ppy content *via* a 4-probe system of a direct current circuit (DC circuit), as shown in (Fig. S3†). Noteworthy, the conductivity of nanocomposites was increased with increasing Ppy content up to 50%, and nanocomposites with Ppy content up to 50% were higher than pure Ppy.

The morphological aspects of Ppy, MMT, organoclay, and Ppy/organoclay nanocomposites were also investigated *via* SEM, as shown in (Fig. 3). The morphology of Ppy, and Na-MMT (Fig. 3(a and b)) resembled a tree-like and flake-like structure, respectively. Moreover, micrographs of the surface of Ppy/organoclay nanocomposites exhibited a cauliflower-like structure with a homogenous dispersion of the mineral domains in the Ppy matrix without the presence of any inorganic aggregations (Fig. 3(c-f)) with round shape domains in the range of 200–600 nm. Notably, micrographs of nanocomposites with 50% of organoclay exhibited more dense structure compared with that of 10%. This proves that the increase in the organoclay% affects the compactness of the materials.

To give direct evidence of the nanometer-scale exfoliation of organoclay in the Ppy matrix, TEM of some nanocomposites was investigated, as shown in (Fig. 4). In [PDM], and [PTM]

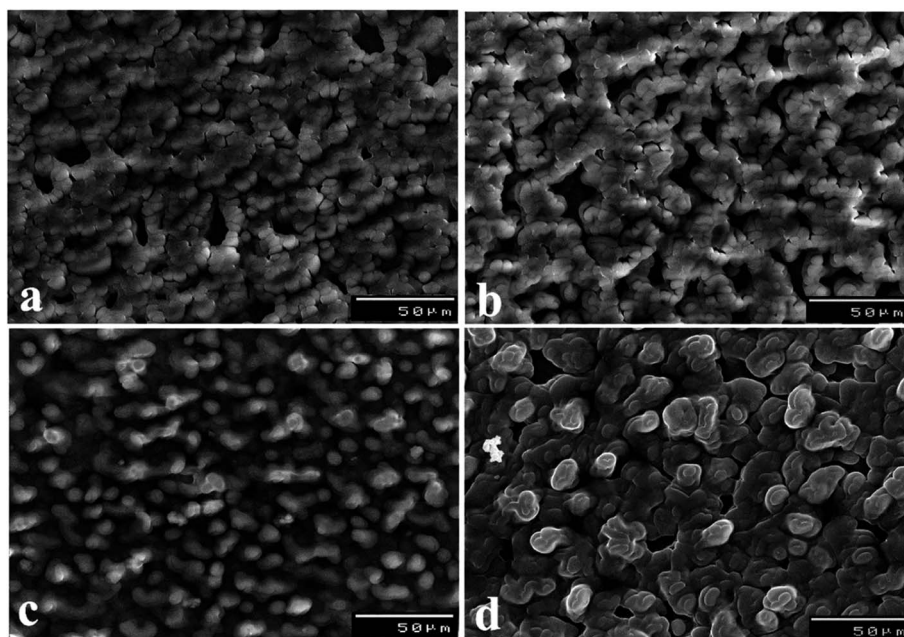


Fig. 2 SEM micrographs of sensor surface with 1.0% of [PT<sub>1</sub>M-50] (a), [PTM-50] (b), [PD<sub>1</sub>M-50] (c), and [PDM-50] (d).



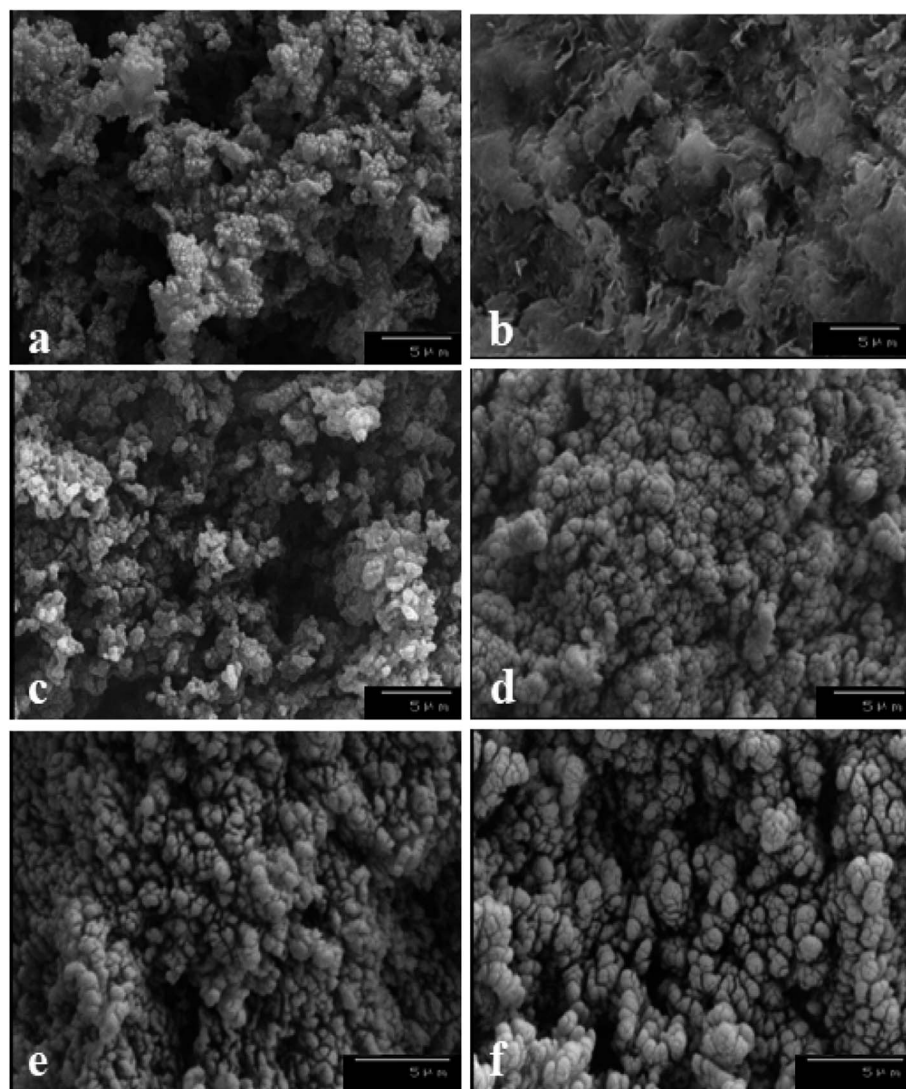


Fig. 3 SEM micrographs of Ppy (a), Na-MMT (b), [PTM-10] (c), [PTM-50] (d), [PDM-10] (e), and [PDM-50] (f) nanocomposites.

nanocomposites, some clay stacks appeared with thickness in the range of 15–100 nm. Since the functional amine groups of polyoxypropylene can form hydrogen bonds with the silicate hydroxylated edge groups, confirming the strong interaction between silicate layers and polymer matrix. Some intercalated organoclay stacks present in the TEM of [PDM-50] (Fig. 4(a)), and [PTM-50] (Fig. 4(b)) micrographs are dispersed uniformly in the matrix. Nanocomposite micrographs revealed a necklace-like shape of organoclay. Meanwhile, the BET analysis (Fig. S4†) indicated that the [PDM-50], and [PTM-50] have a proper specific surface area (SA) of 183.0, and 165.3  $\text{m}^2 \text{g}^{-1}$ , respectively compared with Ppy (28.6  $\text{m}^2 \text{g}^{-1}$ ) and MMT (215.6  $\text{m}^2 \text{g}^{-1}$ ), which confirms the improvements in the geometrical structure of proposed nanocomposites.

### 3.4. Composition, adsorption, affinity, and electrochemical impedance measurements of the constructed sensors

AdAS-SW voltammograms of 30.0 nM NF in pH 5 (B–R buffer) were evaluated upon different compositions (0.5–3.0%) of

[PDM-50] MCPS, as plotted in (Fig. S2(b)†). The maximal peak current was obtained at 1.0% [PDM-50] MCPS, owing to its geometrical structure, as displayed in the SEM micrograph (Fig. 5(b)).

The fabrication of ultrasensitive MCPS does not only depends on the geometrical structure but also mainly on the degree of resistance ( $R_{\text{ct}}$ ) of the sensor. As demonstrated in (Fig. S5†), EIS measurements were evaluated to be 257, and 184  $\Omega$  for [B] CPS, and 1.0% [PDM-50] MCPS, respectively.

Also, the absorption affinity of 10.0 nM NF (pH 5) upon the surface of the [B], and 1.0% [PDM-50] MCPSs were tested, as shown in (Fig. S6†). CVs were recorded at  $E_{\text{acc}} = 0.6 \text{ V}$  for 0.0 s [Cycle (I)], subsequently for 10 s (Cycles 1<sup>st</sup>; (II) and 2<sup>nd</sup>; (III)). In the preceding measurement, a small ox. peak was observed upon the [B] CPS, as shown in (Fig. S6(a)†). While a well-defined peak was revealed upon the 1.0% [PDM-50] MCPS (Cycles 1<sup>st</sup>; (II) and 2<sup>nd</sup>; (III)) (Fig. S5(b)†), which signifies the remarkable enhancements of adsorption property towards NF even at  $t_{\text{acc}} = 0.0 \text{ s}$  [Cycle (I)]. Besides, the noteworthy decay of the peak was



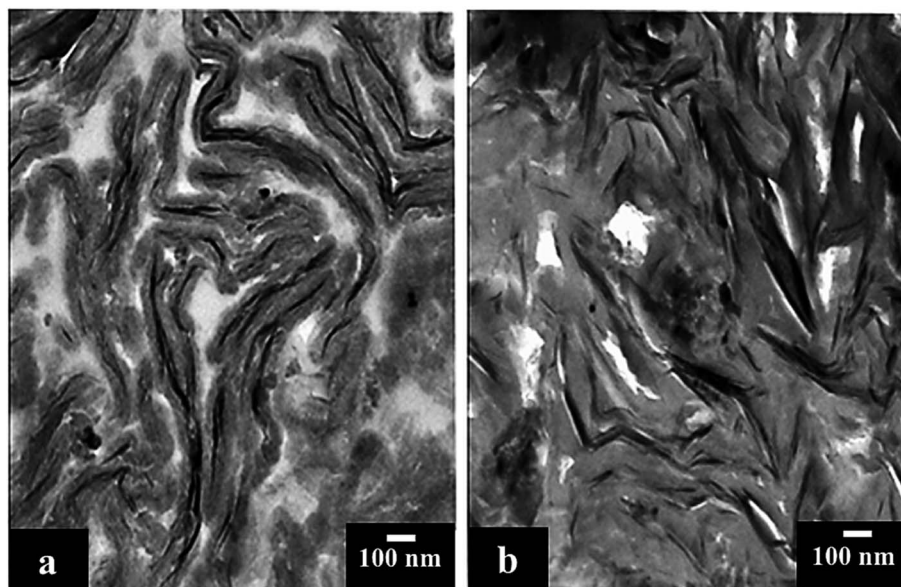


Fig. 4 TEM micrographs of [PDM-50] (a), and [PTM-50] (b).

observed in the [2<sup>nd</sup> cycle; (II)], which denotes the desorption of NF from the surface of the sensor. Therefore, the 1.0% [PDM-50] MCPS has the strongest adsorptive character towards NF with about a 12-time increase in peak current compared with [B] CPS. According to the previous results, 1.0% [PDM-50] MCPS exhibited the highest sensitivity, and adsorption properties for subsequent electroanalytical measurements.

### 3.5. Validation studies

**3.5.1. Adjustment of the analytical parameters.** SW-AdAS voltammograms of 30.0 nM NF were recorded in (pH 2–10) at

$E_{acc} = 0.5$  V for 20 s upon 1.0% [PDM-50] MCPS. As shown in (Fig. S7†), the well-defined peak was obtained at pH 5. Moreover, the optimal pulse, and accumulation parameters were pointed out to be frequency ( $f$ ) = 120 Hz, scan increment ( $\Delta E_s$ ) = 12 mV, pulse height (a) = 30 mV,  $E_{acc} = 0.6$  V for 10 s, as shown in (Fig. S8 and S9†).

**3.5.2. Linearity range, limit of detection, precision, and accuracy.** Under the optimal parameters, SW-AdAS voltammograms of various concentrations of NF have recorded upon 1.0% [PDM-50] MCPS and a linear range of 0.8 to 100 nM with a limit of detection (LOD) of 0.24 nM, as shown in (Fig. 6(A)). As

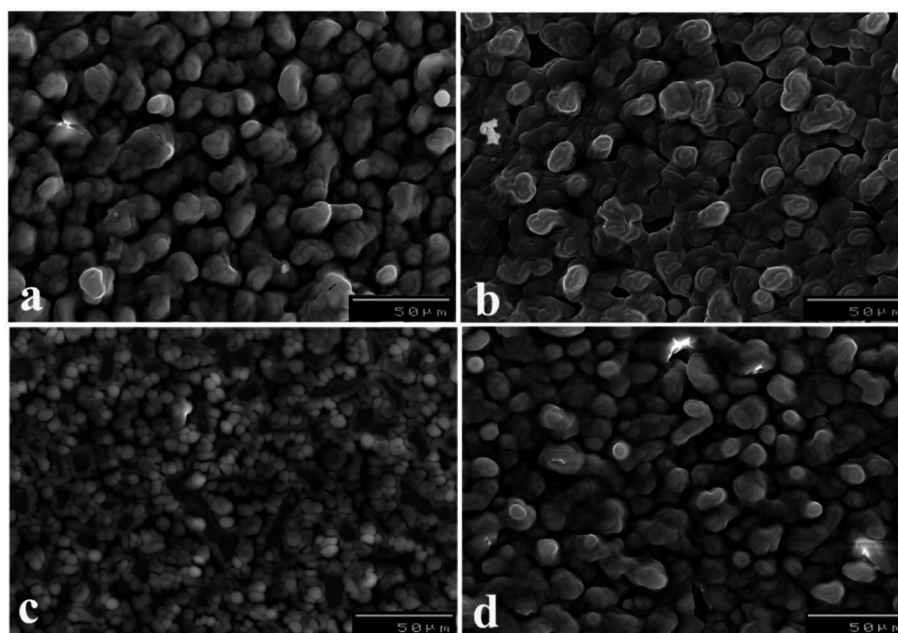


Fig. 5 SEM micrograph of 0.5 (a), 1.0 (b), 2.0 (c), and 3.0% (d) of [PDM-50] MCPSs.





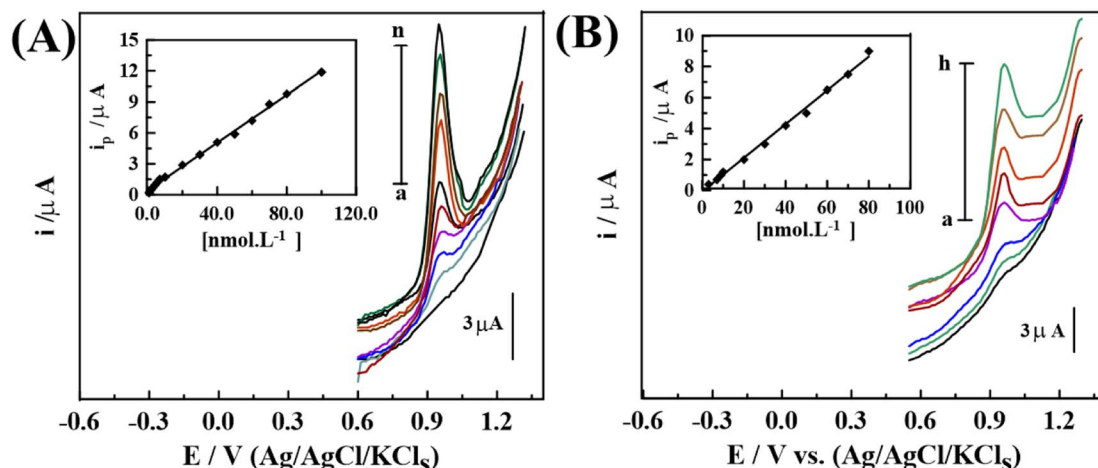


Fig. 6 SW-AdAS voltammograms of various concentrations of NF in pH 5 upon 1.0% [PDM-50] MCPS in (A) bulk: (a) background, (b) 2.0, (c) 6.0, (d) 8.0, (e) 20.0, (f) 30.0, (g) 60.0, (h) 70.0, (i) 80.0 and (j) 100.0 nM of NF and, (B) spiked human urine: (a) background, (b) 7.0, (c) 9.0, (d) 10.0, (e) 30.0, (f) 50.0, (g) 60.0, and (h) 80.0 nM of NF ( $E_{acc} = 0.6$  V for 10 s,  $f = 120$  Hz,  $\Delta E_s = 12$  mV, and  $a = 30$  mV).

Table 2 List of different electrochemical sensors with various voltametric methods for determination of NF<sup>a</sup>

Sensor	Technique	LOD (nM)/LR (nM)	Type of fluid	Ref.
Hg and CPEs	AdSV	36.3	Urine	30
Sephadex-modified CPE	DPV	8.0/15.0–2000	Bulk	26
		50.0–400.0	Urine	
HMDE	HMDE	5.0/100–2000	Bulk	27
		181.7–908.4	Serum	
CNF-SPCEs	LS-AdSV	36.3/1800–10 900	Bulk	29
1.0% [PDM-50] MCPS	SW-AdASV	0.24/0.8–100	Bulk	This work
		0.90/3.0–80	Human urine	

<sup>a</sup> Carbon paste electrode (CPE), differential pulse voltammetry (DPV), linear sweep adsorptive stripping voltammetry (LS-AdSV), carbon nanofiber modified screen-printed electrode (CN-SPCE), adsorptive stripping voltammetry (AdSV), hanging mercury drop electrode (HMDE).

summarized in (Table 2), J. D. Mozo *et al.*<sup>29</sup> recently developed a flow-injection system adsorptive stripping linear sweep voltammetry (LS-AdSV) accompanied by using a screen-printed carbon nanofiber modified electrode (CN-SPC) for determination of NF in the bulk with the LOD of 36.3 nM, followed by recording the NF in numerous commercial tablets only. Noteworthy, the proposed sensor in this work exhibited

a predominant decrease in the value of LOD with about 151-fold in comparison with last reported work<sup>29</sup> and is considered the most sensitive sensor up to date for the detection of NF compared with other tabulated sensors (Table 2). To date, there have been no detailed reports on the usage of SW-AdASV for the sensing of NF drug.

Table 3 Results of intra-day and inter-day analysis of various concentrations of bulk NF by the SW-AdASV method upon 1.0% [PDM-50] MCPS ( $n = 5$ )

Day	[Taken]/(nM)	Mean [found]/(nM)	Recovery (R%)	Accuracy (RE%)	Precision (RSD%)
<b>Intra-day</b>					
1	20.0	20.03	100.15	0.15	1.84
	60.0	60.67	101.12	1.12	0.60
<b>Inter-day</b>					
1	20.0	20.03	100.15	0.15	1.97
	60.0	60.8	101.33	1.33	0.92
2	20.0	20.006	100.03	0.03	2.12
	60.0	60.8	101.33	1.33	0.933
3	20.0	19.773	98.87	−1.13	1.05
	60.0	60.59	100.98	0.98	0.63



In addition, recovery ( $R\%$ ), precision (RSD%), and accuracy (RE%)<sup>68</sup> of the applied SW-AdASV method were estimated by measuring 5 replicates at 3 concentrations levels of bulk NF upon each sensor over 1 day (intra-day), and for 3 days (inter-day), respectively, as shown in (Table 3). There are no significant differences between the taken, and found concentrations of NF. As well as, satisfactory mean ( $R \pm RSD$ ), and RE% were accomplished, confirming the validity of the proposed method for the detection of NF.

**3.5.3. The selectivity, reusability, and stability of the sensor.** As illustrated in (Fig. S10(b)†), the SW-AdAS voltammogram of 20.0 nM NF in the presence of 2.0  $\mu\text{M}$  ( $\sim 100$ -fold) of anionic interferences ( $A_1$ ) including  $\text{Cl}^-$ ,  $\text{PO}_4^{3-}$ ,  $\text{CH}_3\text{COO}^-$ ,  $\text{SO}_4^{2-}$ , and  $\text{CO}_3^{2-}$  was recorded. There is no remarkable change in the magnitude of the voltammetric peak with a recovery ( $R\%$ ) of  $97.95 \pm 2.83\%$ . As well, no extra peaks appeared related to  $A_1^-$  interferences. Furthermore, the magnitude of the SW-AdAS peak current of 20.0 nM NF was estimated in the presence of 20.0 nM of other biological interferences (Mix<sub>1</sub>) such as dopamine (DO), glucose (Glu.) and ascorbic acid (AA), as illustrated in (Fig. S10(c)†). An extra peak has appeared at  $E_p = -0.075$  V, which may be related to (Mix<sub>1</sub>). This peak is far from that of NF that recovery of  $99.13 \pm 1.22\%$  of NF was achieved indicating insignificant interference between them.

On the other hand, the reusability of the sensor was tested by recording five consecutive measurements, which retained 97% of the performance, as shown in (Fig. S11(a)†). After 5 measurements, the performance significantly decreased, owing

to the fullness of the binding cavities on the surface of the sensor. Furthermore, the stability of the sensor was checked by storing the sensor at 4 °C for 1 month accompanied by weekly measurements of the performance. The proposed sensor demonstrated a suitable performance for up to 15 days by retaining its performance up to about 96.3%, as illustrated in (Fig. S11(b)†). After that, the performance decreases gradually up to 90.3% after 30 days. This means that the sensor needs to be stored at a low temperature to avoid damage to the contents of the sensor, and prevent moisture absorption. All these results proved that the sensor has proper selectivity, and sufficient stability for the detection of NF.

### 3.6. Applications

**3.6.1. Assay of NF in medical drug formulation.** The anti-interference ability (selectivity)<sup>68</sup> of 1.0% [PDM-50] MCPS was tested for analysis of solutions of the medical drug of NF (Antinal® and Drotazide® capsules) using SW-AdAS technique in the presence of pharmaceutical drugs (commercial formulations) containing common excipients including starch, lactose, magnesium stearate, glycerin, sucrose, sorbitol, and citric acid. The obtained voltammograms achieved  $R \pm RSD\% \approx 98.00 \pm 1.12$  (Antinal® capsules),  $100.83 \pm 1.24$  (Drotazide® capsules) implied that there is no interference of the frequent excipients drug (Antinal® and Drotazide® capsules) during the detection of NF.

Furthermore, the RSD% of the sensor was pointed out to be 1.12% (Antinal® capsules), and 1.18% (Drotazide® capsules) for 6.0 nM NF utilizing the standard addition method, as illustrated in (Table 4). This result was statistically compared with a reference spectrofluorimetric method.<sup>3</sup> The calculated  $F$ -value did not exceed the theoretical one at the 95.0% confidence level ( $n = 5$ ), and by the  $t$ -test value (Student's  $t$ -test)<sup>69</sup> exhibited non-significant variance in values regarding accuracy and precision. Accordingly, the proposed sensor offered satisfactory recovery in medical drugs even in the presence of drug excipients.

**3.6.2. Assay of nifuroxazide in spiked human urine.** In contrast to the last reported voltammetry measurements,<sup>26,30</sup> a direct and more sensitive detection of NF spiked in human biological fluids was estimated by the optimized method without any medium exchange, and the necessity for extra time for pretreatment or extraction steps before the analysis. Under the standard operational conditions, SW-AdASVs of numerous

**Table 4** Assay of 6.0 nM NF in pharmaceutical drugs by SW-AdASV method in comparison with reference spectrofluorimetric method<sup>3</sup> at the 95% confidence level for  $n = 5$

Method	SW-AdASV method	Reference method
<b>Antinal® capsules</b>		
Mean $C_{\text{found}}/(\text{nM}) \pm \text{SD}$	$5.88 \pm 0.066$	
Mean% recovery $\pm \text{RSD}$	$98.00 \pm 1.12$	$98.44 \pm 1.06$
$F$ -Value	1.12	
$t$ -Test	0.64	
<b>Drotazide® capsules</b>		
Mean $C_{\text{found}}/(\text{nM}) \pm \text{SD}$	$5.98 \pm 0.071$	
Mean% recovery $\pm \text{RSD}$	$99.67 \pm 1.18$	$100.62 \pm 1.12$
$F$ -Value	1.11	
$t$ -Test	1.30	

**Table 5** Results of the calibration curves of the optimized method for the detection of NF in spiking human urine upon 1.0% [PDM-50] MCPS in pH 5 (B–R buffer);  $t_{\text{acc}} = 10$  s,  $E_{\text{acc}} = +0.6$  V,  $f = 120$  Hz,  $\Delta E_s = 12$  mV, and  $a = 30$  mV

Electrode	Linearity range (nM)	$i_p (\mu\text{A}) = (b \pm \text{SD}) C (\mu\text{M}) + (a \pm \text{SD})$	$R^2$	LOD (nM)	LOQ (nM)
Volunteer 1	3.0–80	$i_p = 0.109 \pm 0.35 \times 10^{-3} C - 0.070 \pm 1.90 \times 10^{-2}$	0.998	0.9	3.0
Volunteer 2	3.0–80	$i_p = 0.110 \pm 0.80 \times 10^{-3} C - 0.044 \pm 2.36 \times 10^{-2}$	0.999	0.9	3.0
Volunteer 3	3.5–80	$i_p = 0.106 \pm 1.35 \times 10^{-3} C - 0.042 \pm 2.75 \times 10^{-2}$	0.997	1.05	3.5





concentrations of NF spiked in six human urine samples of 3 healthy volunteers were evaluated (e.g., Fig. 6(B)) upon 1.0% [PDM-50] MCPS. The obtained  $i_p$  of NF upon 1.0% [PDM-50] MCPS was linearly proportional to its concentration over a wide range of 3.0 to 80 nM, as summarized in (Table 5). Notably, no other interfering peaks from other constituents of human urine were detected in the blank sample (e.g., Fig. 6(B), curve (a)). Moreover, satisfactory mean  $R\% = 99.18$ – $102.39$  and  $RSD\% = 0.56$ – $1.17$  of various concentrations of NF in spiked human urine samples were obtained indicating non-significant variance between the added and found concentrations in human urine samples.

Noteworthy, these results revealed that the optimized method upon 1.0% [PDM-50] MCPS has the suitable reliability of direct detection of NF in spiked human urine. As shown in (Table 2), the attained LOD in spiked human urine using 1.0% [PDM-50] MCPS is about 60, and 83 times lower than that in published works by W. Buchberger *et al.*<sup>30</sup> and A. Radi,<sup>26</sup> respectively.

## 4. Conclusion

In this study, we have first introduced a new kind of nano-composite that was used as a modifier for CPS. 1.0% [PDM-50] MCPS shows a remarkable enhancement in the peak current compared with that of bare CPS. The proper reproducibility, wide concentrations ranges and low detection limits in bulk form and urine, make this modified sensor very attractive for assay of NF than other sensors reported in the literature. An additional advantage of the proposed method may be related to its high level of selectivity that allows assay of the NF in the nanomolar level of concentration without the intervention of another compound drug or common excipients. In addition, this method is able to detect the drug in human urine samples without any interference from endogenous materials compared with other published voltammetric methods. Furthermore, the optimized method is rapid, accurate, precise, and economic. The 1.0% [PDM-50] MCPS could be recommended for use in quality control of medical drugs.

## Conflicts of interest

There are no conflicts to declare.

## References

- 1 G. R. Greenstein, *The Merck Index: An Encyclopedia of Chemicals, Drugs, and Biologicals Ref. Rev.*, 2007, **21**, 40.
- 2 H. M. Maher and T. S. Belal, *J. Liq. Chromatogr. Relat. Technol.*, 2012, **35**, 2001–2020.
- 3 T. S. Belal, A simple and sensitive spectrofluorimetric method for analysis of some nitrofurantoin drugs in pharmaceutical preparations, *J. Fluoresc.*, 2008, **18**, 771–780.
- 4 A. A. El-Zaher and M. A. Mahrouse, A validated spectrofluorimetric method for the determination of nifuroxazide through coumarin formation using experimental design, *Chem. Cent. J.*, 2013, **7**, 90.
- 5 A. Abul Khier, M. M. Elhenawee and M. S. Elmasry, Spectrophotometric method for the determination of some drugs using fast red B salt, *J. Chem.*, 2008, **5**, 1087–1097.
- 6 K. Emara, I. Refaat and O. Abdel mageed, HPLC and spectrophotometric determination of nifuroxazide and its pharmaceutical formulations, *Egypt. J. Pharm. Sci.*, 1994, **35**, 313.
- 7 E. Szuminska and A. Cisak, Polarographic and spectrophotometric determination of nifuroxazide in pharmaceuticals. I. Nifuroxazide determination in capsules, *Acta Pol. Pharm.*, 1988, **45**, 551–558.
- 8 E. Szumińska and A. Cisak, Polarographic and spectrophotometric determination of nifuroxazide in pharmaceuticals. II. Determination of nifuroxazide in suspensions, *Acta Pol. Pharm.*, 1990, **47**, 1–2.
- 9 M. I. Toral, M. Paine, P. Leyton and P. Richter, Determination of attapulgit and nifuroxazide in pharmaceutical formulations by sequential digital derivative spectrophotometry, *J. AOAC Int.*, 2004, **87**, 1323–1328.
- 10 F. H. Metwally, M. Abdelkawy and I. A. Naguib, Determination of nifuroxazide and drotaverine hydrochloride in pharmaceutical preparations by three independent analytical methods, *J. AOAC Int.*, 2006, **89**, 78–87.
- 11 F. H. Metwally, Simultaneous determination of nifuroxazide and drotaverine hydrochloride in pharmaceutical preparations by bivariate and multivariate spectral analysis, *Spectrochim. Acta, Part A*, 2008, **69**, 343–349.
- 12 M. A. Hegazy, W. A. Hassanain and L. E. Abdel-Fattah, Stability Indicating Spectrophotometric and Chemometric Methods for Determination of Nifuroxazide in Presence of Its Alkaline Degradation Products, *Pharm. Anal. Acta*, 2011, **2**, 127.
- 13 A. W. Sobanska, Rapid determination of nifuroxazide in tablets by near-infrared spectroscopy, *Chem. Anal.*, 2009, **54**, 1021–1033.
- 14 M. M. Ayad, N. F. Youssef, H. E. Abdellatif and S. M. Soliman, A comparative study on various spectrometries with thin layer chromatography for simultaneous analysis of drotaverine and nifuroxazide in capsules, *Chem. Pharm. Bull.*, 2006, **54**, 807–813.
- 15 P. Guinebault, M. Broquaire and R. Braithwaite, Determination of nifuroxazide in biological fluid by automated high-performance liquid chromatography with large-volume injection, *J. Chromatogr. A*, 1981, **204**, 329–333.
- 16 N. S. Abdelwahab, N. W. Ali, M. M. Zaki, M. Abdelkawy and M. T. El-Saadi, Quantitative Determination of Synthesized Genotoxic Impurities in Nifuroxazide Capsules by Validated Chromatographic Methods, *J. AOAC Int.*, 2018, **101**, 385–393.
- 17 J. Squella, I. Lemus and G. Lonza, Electrochemical study of nifuroxazide and its analytical determination in tablets, *Bol. Soc. Chil. Quim.*, 1991, **36**, 109–116.
- 18 A. Radi, S. El-Laban and I. Kenawy, Determination of nifuroxazide in capsules by differential pulse polarography, *Anal. Sci.*, 1998, **14**, 607–608.



- 19 N. Y. Sreedhar, K. R. Samatha and P. R. K. Reddy, Electrochemical reduction behaviour and analysis of nifuroxazide in formulations and urine samples, *Indian Drugs*, 1999, **36**, 509–512.
- 20 G. R. Naidu, Electrochemical sensing of paracetamol and its simultaneous resolution in the presence of dopamine and folic acid at a multi-walled carbon nanotubes/poly (glycine) composite modified electrode, *Anal. Methods*, 2014, **6**, 9459–9468.
- 21 W. Buchberger, G. Niessner and R. Bakry, Determination of nifuroxazide with polarography and adsorptive stripping voltammetry at mercury and carbon paste electrodes, *Fresenius' J. Anal. Chem.*, 1998, **362**, 205–208.
- 22 A. Radi and M. El Ries, Determination of nifuroxazide in human serum by adsorptive stripping voltammetry, *Anal. Sci.*, 1999, **15**, 385–388.
- 23 J. Mozo, J. Carbajo, J. Sturm, L. Núñez-Vergara, P. Salgado and J. Squella, Determination of Nifuroxazide by Flow Injection Linear Adsorptive Stripping Voltammetry on a Screen-Printed Carbon Nanofiber Modified Electrode, *Electroanalysis*, 2012, **24**, 676–682.
- 24 A. Radi, Voltammetric study of nifuroxazide at unmodified and Sephadex-modified carbon paste electrodes, *Fresenius' J. Anal. Chem.*, 1999, **364**, 590–594.
- 25 J. Squella Serrano, M. Letelier, L. Lindermeier and L. Núñez Vergara, Redox behaviour of nifuroxazide: generation of the one-electron reduction product, *Chem.-Biol. Interact.*, 1996, **99**, 227–238.
- 26 A. Radi, Voltammetric study of nifuroxazide at unmodified and Sephadex-modified carbon paste electrodes, *Fresenius' J. Anal. Chem.*, 1999, **364**, 590–594.
- 27 A. Radi and M. El Ries, Determination of nifuroxazide in human serum by adsorptive stripping voltammetry, *Anal. Sci.*, 1999, **15**, 385–388.
- 28 S. Zayed and Y. J. B. Issa, Cathodic adsorptive stripping voltammetry of drotaverine hydrochloride and its determination in tablets and human urine by differential pulse voltammetry, *Bioelectrochemistry*, 2009, **75**, 9–12.
- 29 J. Mozo, J. Carbajo, J. Sturm, L. Núñez-Vergara, P. Salgado and J. Squella, Determination of Nifuroxazide by Flow Injection Linear Adsorptive Stripping Voltammetry on a Screen-Printed Carbon Nanofiber Modified Electrode, *Electroanalysis*, 2012, **24**, 676–682.
- 30 W. Buchberger, G. Niessner and R. Bakry, Determination of nifuroxazide with polarography and adsorptive stripping voltammetry at mercury and carbon paste electrodes, *Fresenius' J. Anal. Chem.*, 1998, **362**, 205–208.
- 31 M. Elfiky, N. Salahuddin, A. Matsuda, M. Elfiky, N. Salahuddin and A. Matsuda, *Mater. Sci. Eng., C*, 2020, 110773.
- 32 A. Hassanein, N. Salahuddin, A. Matsuda, G. Kawamura and M. Elfiky, Fabrication of biosensor based on chitosan-ZnO/polypyrrole nanocomposite modified carbon paste electrode for electroanalytical application, *Mater. Sci. Eng., C*, 2017, **80**, 494–501.
- 33 A. H. Nagggar, G. A. Saleh, M. A. Omar, A. M. Haredy and S. Derayea, Square wave adsorptive anodic stripping voltammetric determination of antidiabetic drug linagliptin in pharmaceutical formulations and biological fluids using pencil graphite electrode, *Anal. Sci.*, 2020, **36**, 1031–1038.
- 34 L. Pontes, J. De Souza, A. Galembeck and C. De Melo, Gas sensor based on montmorillonite/polypyrrole composites prepared by in situ polymerization in aqueous medium, *Sens. Actuators, B*, 2013, **177**, 1115–1121.
- 35 H. S. El-Desoky, I. M. Ismail and M. M. Ghoneim, Stripping voltammetry method for determination of manganese as complex with oxine at the carbon paste electrode with and without modification with montmorillonite clay, *J. Solid State Electrochem.*, 2013, **17**, 3153–3167.
- 36 H. S. El-Desoky and M. M. Ghoneim, Stripping voltammetric determination of silymarin in formulations and human blood utilizing bare and modified carbon paste electrodes, *Talanta*, 2011, **84**, 223–234.
- 37 G. Kibria and S. Hossain, Electrical resistivity of compacted clay minerals, *Environ. Geotech.*, 2017, **6**, 18–25.
- 38 Z. Yang, W. Wang, X. Tai and G. Wang, Preparation of modified montmorillonite with different quaternary ammonium salts and application in Pickering emulsion, *New J. Chem.*, 2019, **43**, 11543–11548.
- 39 L. Zhang, B. Zhang, T. Wu, D. Sun and Y. Li, Adsorption behavior and mechanism of chlorophenols onto organoclays in aqueous solution, *Colloids Surf., A*, 2015, **484**, 118–129.
- 40 J. L. Alves, P. Rosa and A. R. Morales, A comparative study of different routes for the modification of montmorillonite with ammonium and phosphonium salts, *Appl. Clay Sci.*, 2016, **132**, 475–484.
- 41 L. Wang, S. Liu, T. Wang, D. Sun, L. Wang, S. Liu, T. Wang and D. Sun, *Colloids Surf., A*, 2011, **381**, 41–47.
- 42 J.-J. Lin, I.-J. Cheng, R. Wang and R.-J. Lee, Tailoring basal spacings of montmorillonite by poly (oxyalkylene) diamine intercalation, *Macromolecules*, 2001, **34**, 8832–8834.
- 43 Y. Wang, Y. Duan, Y. Liu and S. Du, Modification of montmorillonite with poly (oxypropylene) amine hydrochlorides: basal spacing, amount intercalated, and thermal stability, *Clays Clay Miner.*, 2011, **59**, 507–517.
- 44 L. Yuzhong, W. Xiaoqun, C. Yichi and D. Shanyi, Co-intercalation of montmorillonite by poly (oxypropylene) amine hydrochlorides with different chain length, *Acta Chim. Sin.*, 2012, **70**, 911–916.
- 45 D. Yifeng, W. Xiaoqun, L. Yuzhong and D. Shanyi, Effect of montmorillonite modified by poly (oxypropylene) amines on curing process of epoxy nanocomposites, *Acta Chim. Sin.*, 2012, **70**, 1179–1186.
- 46 L. Li, H. Zou, M. Liang and Y. Chen, Study on the effect of poly (oxypropylene) diamine modified organic montmorillonite on curing kinetics of epoxy nanocomposites, *Thermochim. Acta*, 2014, **597**, 93–100.
- 47 N. Salahuddin, E. R. Kenawy and R. Abdeen, Polyoxypropylene–montmorillonite nanocomposites for drug-delivery vehicles: preparation and characterization, *J. Appl. Polym. Sci.*, 2012, **125**, E157–E166.



- 48 A. Hassanein, N. Salahuddin, A. Matsuda, T. Hattori and M. Elfiky, Fabrication of electrochemical sensor based on layered double hydroxide/polypyrrole/carbon paste for determination of an alpha-adrenergic blocking agent terazosin, *Electroanalysis*, 2018, **30**, 459–465.
- 49 N. Salahuddin, M. Elfiky and A. Matsuda, Sensors and biosensors nanocomposites based on polymer/inorganic nanostructures, in *Handbook of Polymer Nanocomposites for Industrial Applications*, Elsevier, 2021, pp. 709–731.
- 50 K. Boukerma, J.-Y. Piquemal, M. M. Chehimi, M. Mravčáková, M. Omastová and P. Beaunier, Synthesis and interfacial properties of montmorillonite/polypyrrole nanocomposites, *Polymer*, 2006, **47**, 569–576.
- 51 S. D. Ramôa, G. M. Barra, C. Merlini, W. H. Schreiner, S. Livi and B. G. Soares, Production of montmorillonite/polypyrrole nanocomposites through in situ oxidative polymerization of pyrrole: effect of anionic and cationic surfactants on structure and properties, *Appl. Clay Sci.*, 2015, **104**, 160–167.
- 52 G. Contri, G. Barra, S. Ramoa, C. Merlini, L. Ecco, F. Souza and A. Spinelli, Epoxy coating based on montmorillonite-polypyrrole: electrical properties and prospective application on corrosion protection of steel, *Prog. Org. Coat.*, 2018, **114**, 201–207.
- 53 A. Olad, A. Rashidzadeh and M. Amini, Preparation of polypyrrole nanocomposites with organophilic and hydrophilic montmorillonite and investigation of their corrosion protection on iron, *Adv. Polym. Technol.*, 2013, **32**, 21337.
- 54 Y. Han, Synthesis and characterization of montmorillonite/polypyrrole nanocomposite, *Polym. Compos.*, 2009, **30**, 66–69.
- 55 J. Cuppoletti, *Nanocomposites and Polymers with Analytical Methods*, BoD – Books on Demand, 2011.
- 56 M. Ayad, N. Salahuddin and M. Ali, Polyaniline–organoclay nanocomposites as curing agent for epoxy: preparation and characterization, *Polym. Compos.*, 2009, **30**, 467–473.
- 57 N. Salahuddin, S. Abo-El-Enen, A. Selim and O. S. El-Dien, Synthesis and characterization of polyurethane/organomontmorillonite nanocomposites, *Appl. Clay Sci.*, 2010, **47**, 242–248.
- 58 D. Pospiech, B. Kretschmar, M. Willeke, A. Leuteritz, D. Jehnichen, A. Janke and M. Omastová, Exfoliation behavior of montmorillonite modified by poly(oxyalkylene)s in polypropylene and the properties of the resulting nanocomposites, *Polym. Eng. Sci.*, 2007, **47**, 1262–1271.
- 59 A. M. dos Santos, C. Merlini, S. D. S. Ramôa and G. M. Barra, The Role of Inorganic Fillers in Electrostatic Discharge Composites, *Polym. Compos.*, 2020, **41**, 2003–2012.
- 60 K. Xu, K. Li, D. Tu, T. Zhong and C. Xie, Reinforcement on the mechanical-, thermal-, and water-resistance properties of the wood flour/chitosan/poly (vinyl chloride) composites by physical and chemical modification, *J. Appl. Polym. Sci.*, 2014, **131**, 40757.
- 61 N. Salahuddin, E. R. Kenawy and R. Abdeen, Polyoxypyrrole–montmorillonite nanocomposites for drug-delivery vehicles: preparation and characterization, *J. Appl. Polym. Sci.*, 2012, **125**, E157–E166.
- 62 A. Kassim, H. E. Mahmud and F. Adzmi, Polypyrrole–montmorillonite clay composites: an organic semiconductor, *Mater. Sci. Semicond. Process.*, 2007, **10**, 246–251.
- 63 H. Wu, G. Li and J. Gao, Template synthesis flake polypyrrole and montmorillonite/polypyrrole composites by vapor-liquid phase polymerization, *Acta Mater. Compositae Sin.*, 2009, **26**, 86–92.
- 64 J. Liu and M. Wan, Synthesis, characterization and electrical properties of microtubules of polypyrrole synthesized by a template-free method, *J. Mater. Chem.*, 2001, **11**, 404–407.
- 65 M. Elfiky, R. Kumar and A. Beltagi, Anthropogenic greenhouse CO<sub>2</sub> gas sensor based on glassy carbon modified with organoclay/polypyrrole-alginate nanocomposites in brackish water and seawater, *J. Electroanal. Chem.*, 2022, **926**, 116926.
- 66 K. R. Srinivasan and H. S. Fogler, Use of inorgano-organoclay in the removal of priority pollutants from industrial wastewaters: adsorption of benzo (a) pyrene and chlorophenols from aqueous solutions, *Clays Clay Miner.*, 1990, **38**, 287–293.
- 67 N. L. Dias Filho, D. R. do Carmo, N. L. Dias Filho and D. R. do Carmo, *Talanta*, 2006, **68**, 919–927.
- 68 T. Rao, Validation of analytical methods, *Calibration and Validation of Analytical Methods – A Sampling of Current Approaches*, 2018, pp. 131–141.
- 69 G. D. Christian, Sequential injection analysis for electrochemical measurements and process analysis, *Analyst*, 2014, **119**, 2309–2314.

